Decoupling Network Integrated With CSRR-Based Filtering Power Dividers for Antenna Arrays

Zhang, Yiming ; Li, Xu; Zhang, Shuai; Xiao, Shaoqiu

Published in:
I E E E Transactions on Circuits and Systems. Part 2: Express Briefs

Publication date:
2023

Decoupling Network Integrated With CSRR-Based Filtering Power Dividers for Antenna Arrays

Yi-Ming Zhang, *Member, IEEE,* Xu Li, Shuai Zhang, *Senior Member, IEEE,* and Shao-Qiu Xiao

***Abstract*—This brief provides a mutual coupling suppression network for antenna arrays with high frequency selectivity. The proposed network is composed of three-order (denoting three decoupling bridges established by transmission lines) decoupling networks and unequal power dividers consisting of complementary split-ring resonators featuring bandpass and harmonic suppression responses. All the decoupling structures are highly integrated. A design example of a 2×4 patch antenna array, working at 4.9 GHz and integrated with the proposed decoupling network, is constructed and fabricated. Simulated and measured results indicate that the antenna array is well-decoupled involving the suppression of vertical, horizontal, and diagonal coupling paths. The measured common bandwidth of impedance matching ($|S_{ii}| < -10$ dB) and isolation (> 25 dB) is from 4.8 to 5.1 GHz. A small insertion loss of 0.35 dB is introduced. Moreover, a filtering response is observed, and gain nulls are generated at the two sides of the operating band. As for the demonstrator, spurious up to 11 GHz is well suppressed and the peak gain at the harmonic band is reduced by over 20 dB, exhibiting a good harmonic suppression performance.**

***Index Terms*—Multiple input multiple output antennas, large-scale array, antenna decoupling, bandpass, harmonic suppression.**

I. Introduction

MASSIVE multiple input multiple output (MIMO) antenna systems would be one of the core techniques for future wireless communication systems [1]-[3]. The technique features the ability of beam scanning in three dimensions, such as covering vehicles, drones, ships, civil airliners, and even low-orbit satellites. However, the strong coupling between the elements in the massive MIMO antenna arrays would significantly worsen the active impedance matching performance, bring non-linear distortion on power amplifiers, and increase the error rate of MIMO communication systems [4]-[6]. Therefore, mutual coupling suppression between antennas is of great importance and has been widely studied recently [7]-[15].

This work was supported by the Guangdong Basic and Applied Basic Research Foundation under Grant 2023A1515011412. (Corresponding author: Shao-Qiu Xiao)

Yi-Ming Zhang, Xu Li, and Shao-Qiu Xiao are with the School of Electronics and Information Technology, and Guangdong Provincial Key Laboratory of Optoelectronic Information Processing Chips and Systems, Sun Yat-Sen University, China. (email: zhangyim9@mail.sysu.edu.cn, lixu53@mail2.sysu.edu.cn, xiaoshq8@mail.sysu.edu.cn)

Shuai Zhang is with the Antenna, Propagation and Millimeter-wave Systems (APMS) Section, Department of Electronic Systems, Aalborg University, 9220 Aalborg, Denmark (e-mail: sz@es.aau.dk).

Color versions of one or more of the figures in this article are available online at http://ieeexplore.ieee.org

Decoupling methods operated at feeding layer feature a low profile and small influence on radiation performance since the decoupling structures are separated from the radiating parts by ground planes, such as the studies given in [10]-[12]. These decoupling networks characterize good coupling cancellation at the operating bands. However, the out-of-band coupling might be even increased after decoupling. As for the out-of-band coupling, a solution of integrating the decoupling with the filtering concept might be effective. Some specified designs of filtering antennas with coupling suppression were reported in [13]-[15]. These decoupling-filtering schemes verify the feasibility of the combination of decoupling and filtering to reduce both the in-band and out-of-band mutual coupling but still need further investigation or improvement in spurious suppression bandwidth, applicable array configuration, and other aspects.

In this brief, a decoupling method is proposed for 2×*N* antenna arrays. Different from the one given in [12], the proposed method does not require identical diagonal coupling levels, and is not limited by the condition that the diagonal coupling paths should be weaker than other paths. An unequal power divider reported in [16], using complementary split-ring resonators (CSRRs), is employed to construct the decoupling bridge. It is found in this work that the unequal CSRR power divider features a harmonic suppression response which was not mentioned in [16], leading to the decoupling, bandpass filtering, and harmonic suppression simultaneously.

II. Decoupling and Filtering Method

Illustrated in Fig.1 is a 2×*N* antenna array consisting of 45º-polarized antenna elements. Four non-marginal and adjacent elements are selected as the representative elements. Due to the array arrangement and polarization direction, the mutual coupling levels of horizontal (*path a*), vertical (*path b*), and two diagonal (*paths c* and *d*) paths would be different. Particularly, the coupling through two diagonal paths has an apparent discrepancy. Here, a three-order CSRR-based decoupling network is given to cancel the four different coupling paths for 2×*N* antenna arrays.

A. Analysis of the Proposed Decoupling Network

Shown in Fig. 2 is the block diagram of the proposed decoupling network composed of CSRR-based unequal power dividers and three-order decoupling bridges. For ease of describing the principle, the decoupling network is split into two aspects (common and specified parts) by using the signal flow graph, as shown in Fig. 3. The common part is described in Fig. 3(a), consisting of four common nodes, marked as

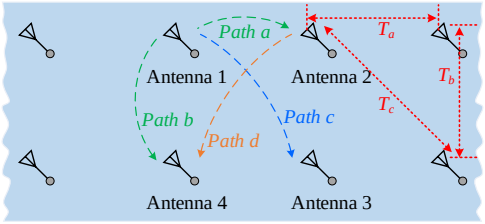

Fig. 1. Mutual coupling diagram within a 45º- polarized 2×N antenna array.

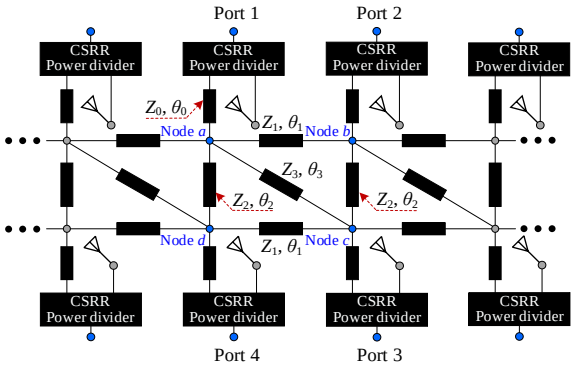

Fig. 2. Block diagram of the proposed CSRR-based decoupling network.

Nodes 1, 2, 3 and 4. The parameter S_{MC} is the coupling coefficient between two adjacent elements (vertical, horizontal, or diagonal direction), located between Nodes 3 and 4. The parameters $S_{PD,\,1}$ and $S_{PD,\,2}$ are the transmission coefficients from the input port of the CSRR-based power divider to the two output ports, which are connected with antennas and decoupling bridges, respectively.

For the four coupling paths mentioned in Fig. 1, four equivalent decoupling paths, i.e., the specified parts, are established using a signal flow graph, as illustrated in Fig. 3. The parameters $S_{N,\,ij}$ are the S parameters of a five-port network given in Fig. 4 which is a simplified circuit to approximately describe the transmission responses through the common nodes (Nodes a, b, c, and d) shown in Fig. 1. According to the transmission line theory, the values of $S_{N,\,ij}$ (recorded in dB) can be expressed as

$$S_{N,21}^{dB} = S_{N,12}^{dB} = 20\log\left[\frac{2\sqrt{Z_0 Z_1}}{Z_1 + Z_0\left(\frac{1}{Z_1}+\frac{1}{Z_2}+\frac{1}{Z_3}+1\right)}\right] \tag{1a}$$

$$S_{N,31}^{dB} = S_{N,13}^{dB} = 20\log\left[\frac{2\sqrt{Z_0 Z_3}}{Z_3 + Z_0\left(\frac{2}{Z_1}+\frac{1}{Z_2}+1\right)}\right] \tag{1b}$$

$$S_{N,41}^{dB} = S_{N,14}^{dB} = 20\log\left[\frac{2\sqrt{Z_0 Z_2}}{Z_2 + Z_0\left(\frac{2}{Z_1}+\frac{1}{Z_3}+1\right)}\right] \tag{1c}$$

where Z_0 is the output impedance of the CSRR power divider. To avoid reflection between the output of the CSRR power divider and Node a, we set $|S_{N,11}|$=0, indicating that

$$\frac{1}{Z_0} = \frac{2}{Z_1} + \frac{1}{Z_2} + \frac{1}{Z_3} \tag{2}$$

Based on the discussions, the magnitude relationships of coupling and decoupling paths can be obtained between Ants. 1 and 2, Ants. 1 and 4, Ants. 1 and 3, given as

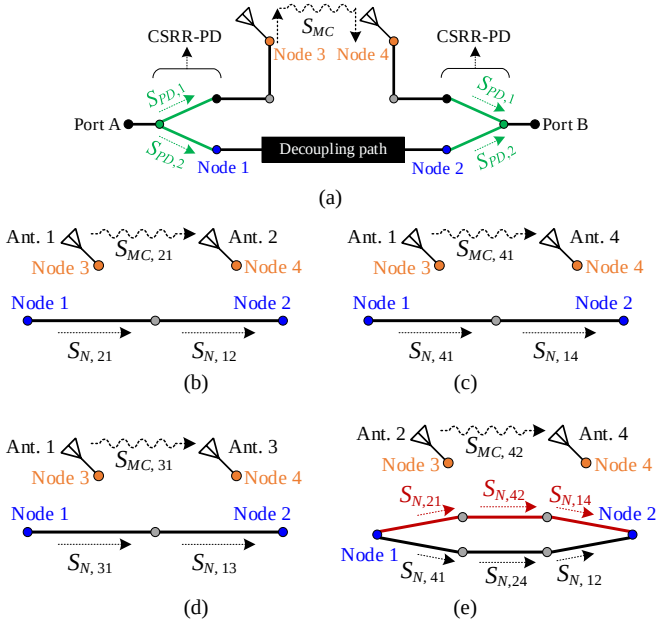

Fig. 3. Signal flow graphs of the representative elements integrated with the proposed decoupling network. (a) Common part. Specified parts for suppressing the mutual coupling between (b) Antennas 1 and 2, (c) Antennas 1 and 4, (d) Antennas 1 and 3, (e) Antennas 2 and 4.

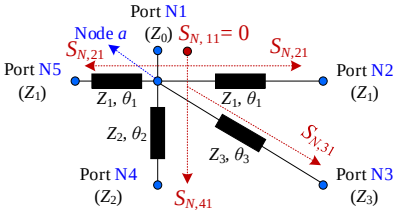

Fig. 4. Simplified circuit model for approximately describing the transmission coefficients through Node a marked in Fig. 2.

$$S_{PD,1}^{dB} + S_{MC,21}^{dB} + S_{PD,1}^{dB} = S_{PD,2}^{dB} + 2S_{N,21}^{dB} + S_{PD,2}^{dB} \tag{3a}$$

$$S_{PD,1}^{dB} + S_{MC,41}^{dB} + S_{PD,1}^{dB} = S_{PD,2}^{dB} + 2S_{N,41}^{dB} + S_{PD,2}^{dB} \tag{3b}$$

$$S_{PD,1}^{dB} + S_{MC,31}^{dB} + S_{PD,1}^{dB} = S_{PD,2}^{dB} + 2S_{N,31}^{dB} + S_{PD,2}^{dB} \tag{3c}$$

where the superscript "dB" denotes that the parameters are in the dB description. Although there is no direct decoupling bridge located between Ants. 2 and 4, the mutual coupling can also be suppressed through the decoupling paths illustrated in Fig. 3(e), formulated as

$$S_{PD,1}^{dB} + S_{MC,42}^{dB} + S_{PD,1}^{dB} = S_{PD,2}^{dB} + S_{N}^{dB} + S_{PD,2}^{dB} \tag{4a}$$

$$S_{N}^{dB} = 20\log\left|S_{N,21}S_{N,42}S_{N,14} + S_{N,41}S_{N,24}S_{N,12}\right| \tag{4b}$$

The coupling coefficients $S_{MC,\,21}$, $S_{MC,\,41}$ $S_{MC,\,31}$, and $S_{MC,\,42}$ can be obtained from full-wave simulations. Further, since

$$S_{N,21} = S_{N,12},\quad S_{N,41} = S_{N,14},\quad S_{N,24} = S_{N,42} \tag{5}$$

The relationship expressed in (4) can be simplified, given as

$$\begin{aligned} S_{PD,1}^{dB} + S_{MC,42}^{dB} + S_{PD,1}^{dB} &= S_{PD,2}^{dB} \\ &+ 20\log 2 + S_{N,21}^{dB} + S_{N,42}^{dB} + S_{N,41}^{dB} + S_{PD,2}^{dB} \end{aligned} \tag{6}$$

The above derivation provides the magnitude conditions of the decoupling paths. The characteristic impedance of Z_1, Z_2, and Z_3, and the power division (regarding $S_{PD,\,1}$ and $S_{PD,\,2}$) of the CSRR-based power divider can be determined through (1)-(6). Next, the phase condition will be given. The initial values of

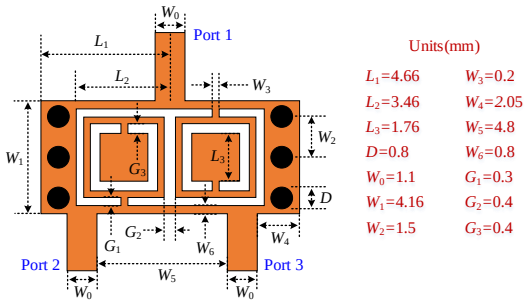

Fig. 5. Configuration of the CSRR-based unequal power divider given in [16], working at 4.9 GHz. Substrate Rogers RO4350B is used, with a permittivity of 3.66 and thickness of 0.508 mm.

the electrical lengths θ_1, θ_2, and θ_3 are set as

$$\theta_1 = 2\pi\frac{T_a}{\lambda_g},\quad \theta_2 = 2\pi\frac{T_b}{\lambda_g},\quad \theta_3 = 2\pi\frac{T_c}{\lambda_g} \tag{7}$$

where λ_g is the waveguide wavelength at the center frequency. As marked in Fig.1, the parameters T_a, T_b, and T_c are the physical distances between the vertical, horizontal, and diagonal located elements, correspondingly. It is seen in Fig. 1 that there is an additional transmission line characterizing with Z_0 and θ_0, which is employed for compensating and adjusting the phase difference between the original coupling and decoupling paths. To generate decoupling paths, we have

$$\left|S_{PD,1}^{Pha}\right| + \left|S_{MC,21}^{Pha}\right| + \left|S_{PD,1}^{Pha}\right| = \left|S_{PD,2}^{Pha}\right| + 2\theta_0 + \theta_1 + \left|S_{PD,2}^{Pha}\right| \tag{8a}$$

$$\left|S_{PD,1}^{Pha}\right| + \left|S_{MC,41}^{Pha}\right| + \left|S_{PD,1}^{Pha}\right| = \left|S_{PD,2}^{Pha}\right| + 2\theta_0 + \theta_2 + \left|S_{PD,2}^{Pha}\right| \tag{8b}$$

$$\left|S_{PD,1}^{Pha}\right| + \left|S_{MC,31}^{Pha}\right| + \left|S_{PD,1}^{Pha}\right| = \left|S_{PD,2}^{Pha}\right| + 2\theta_0 + \theta_3 + \left|S_{PD,2}^{Pha}\right| \tag{8c}$$

$$\left|S_{PD,1}^{Pha}\right| + \left|S_{MC,42}^{Pha}\right| + \left|S_{PD,1}^{Pha}\right| = \left|S_{PD,2}^{Pha}\right| + 2\theta_0 + \theta_1 + \theta_2 + \left|S_{PD,2}^{Pha}\right| \tag{8d}$$

where the superscript "*Pha*" denotes that the *S* parameters are in the "Phase" description. Finally, the mutual coupling can be well-canceled, where the parameters Z_1, Z_2, Z_3, θ_0, θ_1, θ_2, and θ_3 can be determined. Here, the power division of the CSRR-based power divider is also derived. Next, the physical layout of the power divider will be determined.

B. Determination of CSRR-Based Power Divider

The CSRR-based unequal power divider with bandpass response reported in [16] is utilized in this work. As shown in Fig.5, the power divider consists of two parallelly positioned CSRRs with rotational symmetry. As discussed in [16], a wide-range power division ratio can be achieved by changing the position (W_4) of the output ports and the distance (W_5) between the two output ports. For ease of analysis, we give an example working at 4.9 GHz with a power ratio of around 1:4, whose dimensions are listed in Fig. 5. Fig. 6(a) illustrates the impedance matching at the input port, and the phase and magnitude imbalance between the output ports at 4.9 GHz are also given, against different values of W_3. It is found that the phase difference is stable and kept around 9º. The magnitude difference can be tuned within a wide range, as expected.

Seeing that the power division ratio is given through the above derivation, under the decoupling conditions. The final layout of the CSRR-based power divider can be readily determined. Moreover, we found that the unequal power divider features a harmonic suppression response, which was

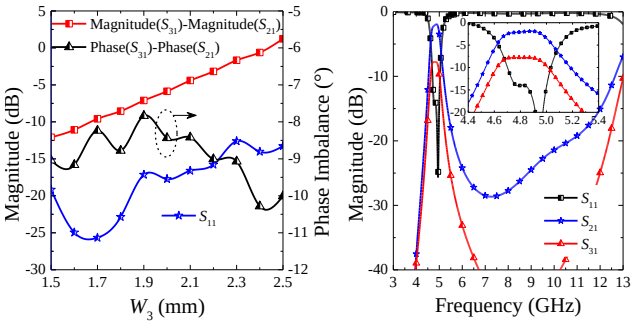

Fig. 6. (a) Transmission responses of the CSRR-based unequal power divider against different values of W_3. (b) Full-wave simulated results of an unequal power divider working at 4.9 GHz with a power ratio around 1:4.

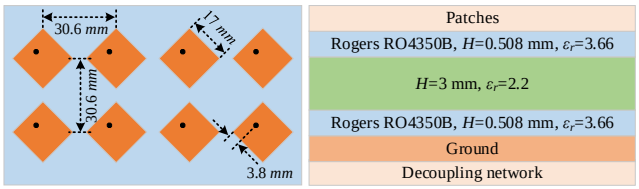

Fig. 7. Configuration of a 2×4 patch antenna array integrated with the proposed decoupling network.

not mentioned in [16]. It is seen that the out-of-band spurious of up to 11 GHz are suppressed to less than –19 dB. Fig. 6(b) shows the simulated *S* parameters of the CSRR-based 1:4 unequal power divider, which features a bandpass response with harmonic suppression, as expected.

C. Design Example

For demonstration purposes, a 2×4 patch antenna array working at 4.9 GHz and integrated with the proposed decoupling network is developed, as shown in Fig. 7. The numerically determined values of the parameters are: Z_1 = 55.8 Ω, Z_2 = 83.8 Ω, Z_3 = 108.6 Ω, θ_0 = 91.4º, θ_1 = 280.6º, θ_2 = 284.3º, θ_3 = 411.7º, and the output ratio of the CSRR-based power divider is 1:3.85. After full-wave simulation and post-optimization to reduce the effects of meandered lines and soldering pads for realization, the final layout of the decoupled antenna array can be established.

III. Measurement and Discussion

Shown in Fig. 8(a) is the fabricated 2×4 patch antenna array loading with the proposed decoupling network. The measured *S* parameters of the decoupled array are shown in Figs. 8(b)-8(d), where Port 2 is selected as the representative port. The impedance-matching bandwidth of the decoupled array is from 4.7 to 5.1 GHz. The measured magnitude of S_{11} is kept higher than –0.9 dB at out of band up to 11 GHz, while that of the array without decoupling is lower than –8.8 dB. This denotes that a bandpass response with harmonic suppression is achieved. Fig. 8(c) shows the in-band coupling levels between the elements located along the *x*- and *y*-axis, i.e., S_{32}, and S_{62}, which are suppressed from –16.7 dB to less than –25 dB within the operating band. As for the E- and H-coupling paths, i.e., S_{52}, and S_{72}, they are also canceled as expected. The out-of-band coupling between Port 2 and other ports is provided, as shown in Fig. 9. It is seen that the out-of-band coupling of the array without

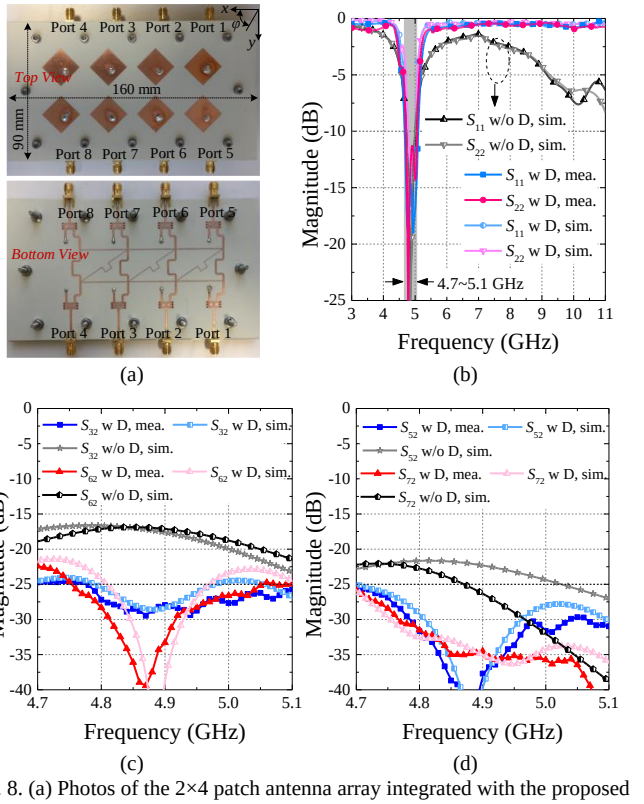

Fig. 8. (a) Photos of the 2×4 patch antenna array integrated with the proposed decoupling structure. (b) S_{11} and S_{22}, (c) S_{32} and S_{62}, (d) S_{52} and S_{72} of the decoupled antenna array.

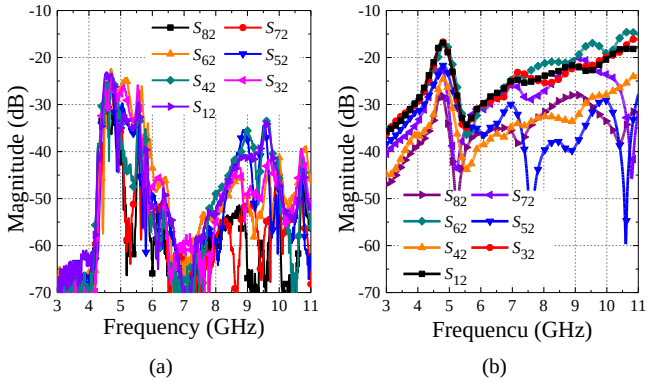

Fig. 9. Mutual coupling between Port 2 and other ports of (a) the decoupled antenna array and (b) the array without decoupling.

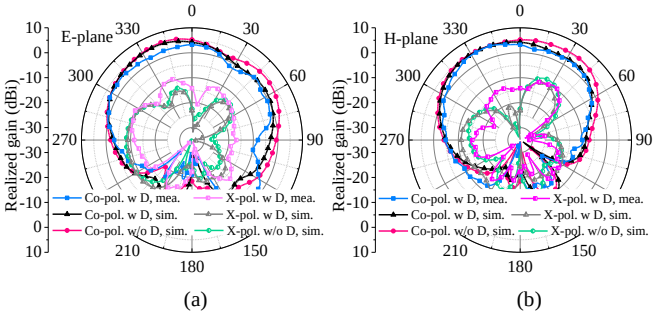

Fig. 10. Radiation patterns of the array with and without decoupling when Port 2 is excited. (a) E-plane. (b) H-plane.

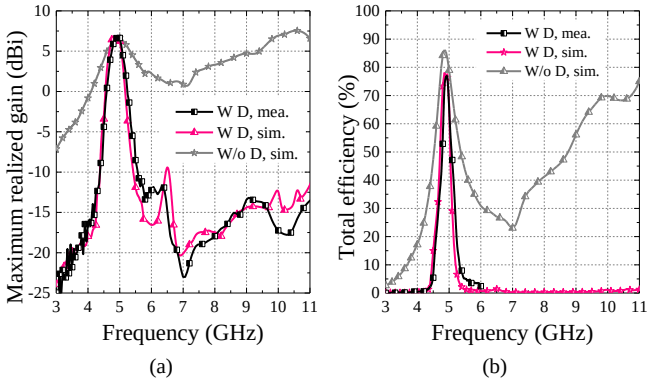

Fig. 11. (a) Peak gain and (b) total efficiency of the array with and without decoupling when Port 2 is excited.

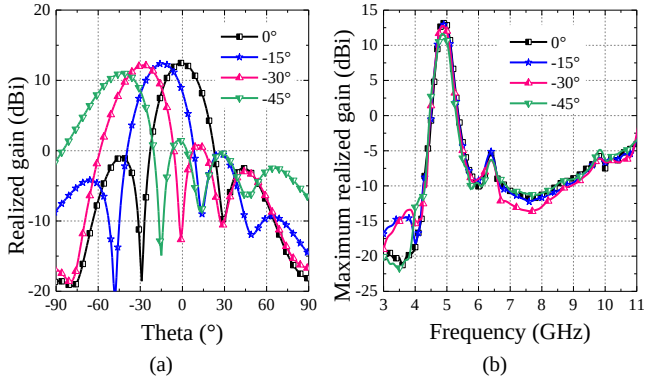

Fig. 12. (a) Simulated beam-scanning performance of the decoupled 2×4 antenna array at the cut of φ=0º. (b) Simulated maximum realized gain of the decoupled 2×4 antenna array under different beam directions.

decoupling is strong, higher than –15 dB, which is suppressed to less than –25 dB among the entire studied band after decoupling.

The far-field radiation performance is given in Figs. 10 and 11. The radiation patterns are almost not influenced after decoupling. The in-band peak gain of the decoupled antenna is over 6.6 dBi. As for the total efficiency of the decoupled array, slight degradation from 86.2% to 78.3% is found, indicating a small insertion loss of 0.35 dB. Despite that, the radiation performance is acceptable. Note that limited by the measurement platform, the total efficiency is not tested beyond 6 GHz. The full-wave simulation shows that the out-of-band (up to 12 GHz) total efficiency of the decoupled array is less than 5%, while that of the coupling array is over 70% at the harmonic frequency.

The stability of the frequency selectivity of the decoupling array under beam scanning conditions is also discussed by using full-wave simulations. Four beams at φ=0º plane with different directions are formed at 4.9 GHz, as shown in Fig. 12(a). The peak gain of the beams within the range from 3 to 12 GHz is illustrated in Fig. 12(b) where the out-of-band gains are suppressed to low levels. Note that at φ=90º plane, beam scanning can be also enabled by exciting the elements at different rows under different phases. However, the scanning angle is not as large as the one operating at φ=90º plane, owing to the limited rows. The active impedance matching performance of the arrays with and without decoupling is provided in Fig. 13 with the scanning beam of –45º. It is seen the elements of the decoupled array are well matched. However, as for the array without coupling, the ports are almost mismatched within the operating band when the beam is with a large scanning angle, and strong spurious at the harmonic frequencies are generated. Therefore, it can be concluded that the filtering responses are not sensitive to beam scanning. To clearly show the advantages of the proposed decoupling network, some recently

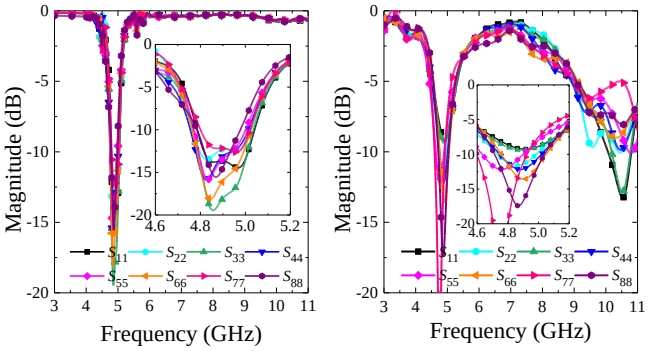

Fig. 13. Simulated active reflection coefficients of the antenna arrays under beam-scanning conditions. (a) With decoupling. (b) Without decoupling.

TABLE I
PERFORMANCE COMPARISON BETWEEN THE PROPOSED AND RECENTLY PUBLISHED DECOUPLING SCHEMES

Ref.	Array configuration	Bandpass response	Harmonic suppression	Profile
[7]/2022	2×2	*NO*	*NO*	0.052λ
[8]/2022	*M*×*N*	*NO*	*NO*	0.49λ
[9]/2020	1×2	*NO*	*NO*	0.018λ
[12]/2019	*M*×*N*	*NO*	*NO*	0.212λ
[14]/2022	1×2	*YES*	*NO*	0.022λ
[15]/2021	*M*×*N*	*YES*	*NO*	0.09λ
This work	**2×*N***	***YES***	***YES***	**0.066λ**

published decoupling methods are summarized, as listed in Table I. It is seen that the proposed decoupling method is the one that features bandpass and harmonic suppression response, with low insertion loss and low profile.

IV. CONCLUSION

A decoupling network consisting of transmission-line-based decoupling bridges and CSRR-based unequal power dividers is proposed in this work for large-scale antenna arrays, particularly, for 45º-polarized antenna arrays where the diagonal coupling paths are not identical since E- and H-coupling are both involved. Theoretical analysis, full-wave simulation, and measurement are provided to verify and demonstrate the performance of the proposed scheme. In this work, the CSRR-based power divider not only serves as a part of the decoupling bridges but also provides the functions of impedance matching, filtering, as well as harmonic suppression. This makes the proposed scheme valuable and attractive for highly integrated multi-functional large-scale antenna systems.

REFERENCES

[1] B. He, A. Zhang, W. Hao, P. Liu, and B. Ning, "Multiple beam selection and near-optimal digital precoding for multiuser millimeter-wave massive MIMO systems," *IEEE Transactions on Circuits and Systems II: Express Briefs*, vol. 70, no. 2, pp. 811-815, Feb. 2023.

[2] G. R. Nikandish, R. B. Staszewski, and A. Zhu, "A fully integrated GaN dual-channel power amplifier with crosstalk suppression for 5G massive MIMO transmitters," *IEEE Transactions on Circuits and Systems II: Express Briefs*, vol. 68, no. 1, pp. 246-250, Jan. 2021.

[3] X. Tan, H. Han, M. Li, K. Sun, Y. Huang, X. You, and C. Zhang, "Approximate expectation propagation massive MIMO detector with weighted Neumann-series," *IEEE Transactions on Circuits and Systems II: Express Briefs*, vol. 68, no. 2, pp. 662-666, Feb. 2021.

[4] L. Savy and M. Lesturgie, "Coupling effects in MIMO phased array," in *Proc. IEEE Radar Conf. (RadarConf)*, Philadelphia, PA, USA, May 2016, pp. 1–6.

[5] K.-H. Chen and J.-F. Kiang, "Effect of mutual coupling on the channel capacity of MIMO systems," *IEEE Transactions on Vehicular Technology*, vol. 65, no. 1, pp. 398–403, Jan. 2016.

[6] X. Chen, S. Zhang, and Q. Li, "A review of mutual coupling in MIMO systems," *IEEE Access*, vol. 6, pp. 24706–24719, 2018.

[7] P. Kumar, S. Pathan, S. Vincent, O. P. Kumar, Yashwanth N, P. Kumar, P. R. Shetty, and T. Ali, "A compact quad-port UWB MIMO antenna with improved isolation using a novel mesh-like decoupling structure and unique DGS," *IEEE Transactions on Circuits and Systems II: Express Briefs*, vol. 70, no. 3, pp. 949-953, March 2023.

[8] S. Luo, G. F. Pedersen and S. Zhang, "Massive MIMO array design with high isolation by using decoupling cavity," *IEEE Transactions on Circuits and Systems II: Express Briefs*, vol. 70, no. 3, pp. 974-978, March 2023.

[9] P. Garg and P. Jain, "Isolation improvement of MIMO antenna using a novel flower shaped metamaterial absorber at 5.5 GHz WiMAX Band," *IEEE Transactions on Circuits and Systems II: Express Briefs*, vol. 67, no. 4, pp. 675-679, April 2020.

[10] A. A. Diman, F. Karami, P. Rezaei, A. Amn-e-Elahi, Z. Mousavirazi, T. A. Denidni, and A. A. Kishk, "Efficient SIW-feed network suppressing mutual coupling of slot antenna array," *IEEE Transactions on Antennas and Propagation*, vol. 69, no. 9, pp. 6058-6063, Sept. 2021.

[11] M. Li, Y. Zhang, D. Wu, K. L. Yeung, L. Jiang and R. Murch, "Decoupling and matching network for dual-band MIMO antennas," *IEEE Transactions on Antennas and Propagation*, vol. 70, no. 3, pp. 1764-1775, March 2022.

[12] Y.-M. Zhang, S. Zhang, J.-L. Li, and G. F. Pedersen, "A transmission-line-based decoupling method for MIMO antenna arrays", *IEEE Transactions on Antennas and Propagation*, vol. 67, no. 5, pp. 3117-3131, May 2019.

[13] S. J. Yang, W. Duan, Y. Y. Liu, H. Ye, H. Yang and X. Y. Zhang, "Compact dual-band base-station antenna using filtering elements," *IEEE Transactions on Antennas and Propagation*, vol. 70, no. 8, pp. 7106-7111, Aug. 2022.

[14] M. Li, S. Tian, M. -C. Tang and L. Zhu, "A compact low-profile hybrid-mode patch antenna with intrinsically combined self-decoupling and filtering properties," *IEEE Transactions on Antennas and Propagation*, vol. 70, no. 2, pp. 1511-1516, Feb. 2022.

[15] Y.-M. Zhang, Q.-C. Ye, G. F. Pedersen, and S. Zhang, "A simple decoupling network with filtering response for patch antenna arrays", *IEEE Transactions on Antennas and Propagation*, vol. 69, no. 11, pp. 7427-7439, Nov. 2021.

[16] M. Danaeian, A.-R. Moznebi, K. Afrooz, and H. Hakimi, "Miniaturised equal/unequal SIW power divider with bandpass response loaded by CSRRs", *Electronics Letters*, vol. 52, no. 22, pp. 1864-1866, Oct. 2016.